IOP Conf. Series: Earth and Environmental Science **240** (2019) 032026 doi:10.1088/1755-1315/240/3/032026

PIV measurement of internal flow in mini centrifugal pump

T Shigemitsu[1], Y Ogawa[2] and E Nakaishi[2]

[1] Institute of Science and Technology, Tokushima University, 2-1 Minamijyosanjima-cho, Tokushima-city, 770-8506, JAPAN
t-shige@tokushima-u.ac.jp

[2] Graduate School of Advanced Technology and Science, Tokushima University
2-1 Minamijyosanjima-cho, Tokushima-city, 770-8506, JAPAN
c501732006@tokushima-u.ac.jp

Abstract. The diameter of the ventricular assist pump and cooling pump for electrical devices like servers is about a dozen millimetres and these kinds of pumps belong to the mini pump. The internal flow condition of the mini centrifugal pump has to be clarified because there are so many types of mini pumps according to special specifications and shapes. Therefore, in this research, an open impeller was adopted as a mini centrifugal pump with 55mm impeller diameter in consideration of reduction in impeller manufacturing cost and its internal flow was investigated. Since the outlet angle of the test impeller is large, the maximum efficiency flow rate moves to a large flow rate and the relatively high head and efficiency were obtained in large flow rate region. In the present paper, the velocity and vorticity distribution near the volute tongue are shown and the internal flow in the mini centrifugal pump is clarified based on the PIV measurement results.

1. Introduction

Pumps are widely used in the industrial field and are expected to be applied to the fuel cells and medical devices in recent years [1,2]. Especially, the research related to the ventricular assist pump has been conducted actively all over the world. Some of the researchers represent significant breakthrough for the trouble like the blood clot, which occurs when the mini centrifugal pump is used for the ventricular assist pump, by the adoption of the magnetically suspended pump. Then, the ventricular assist devices are in practical use in USA, Europe, Japan and et al. using the magnetically suspended pump. In addition to that, experimental investigations of the internal flow condition of the ventricular assist pump have been conducted with the numerical analysis [3,4]. Keller et al. investigated the unsteady flow condition inside the volute of the centrifugal pump by PIV measurement and clarified the vortex structure near the volute tongue with the rotation of the impeller [5]. The blade-to-blade flow condition was measured using PIV by Zhang et al. and showed the internal flow of the low specific speed centrifugal pump [6]. Diameter of the ventricular assist pump and cooling pump for servers is less than 100mm and these kinds of pumps belong to the mini pump. Therefore, there are many cases that the conventional design standard and theory can’t be applied due to the small size of the pump and the design method is not established [7]. It was clarified by Nishi et al. that the performance of the mini centrifugal pump based on the conventional design method using the closed impeller was better than that using the open impeller. However, it is considered that the open impeller is suitable for the mini centrifugal pump on the point of view of the maintenance of the pump and the manufacture of the impeller. On the other hand, it was also verified by Nishi et al. that adequate performance could be obtained even in the open impeller designed by the original design method, in which the blade outlet angle and blade number were increased [8-10]. The two dimensional impeller is often used for the mini centrifugal pump because the mini centrifugal pump can't fully demonstrate the advantages concerning the performance of the three dimensional impeller. Furthermore, the mini centrifugal pump has a tendency getting lower specific speed with the high head and low flow rate. It was clarified that the sufficient performance could be obtained with the two dimensional impeller under the condition of the low specific speed [11]. Therefore, the two dimensional open impeller was adopted as a mini centrifugal pump with 55mm impeller diameter in consideration of reduction in impeller manufacturing cost. Then, the internal flow of this test pump was investigated by PIV measurement.

In the present paper, the internal flow near the casing tongue is clarified using the mini centrifugal pump having the 55mm impeller diameter. The internal flow near the casing tongue of the PIV measurement is compared with the numerical analysis results to evaluate the validity of the PIV measurement results. The vortex structure near the casing tongue was visualized by the PIV measurement results when the trailing edge of the impeller approaching and leaving the casing tongue.

2. Experimental apparatus

2.1. Design specification and experimental apparatus for performance test

A test rotor of the mini centrifugal pump was designed based on the conventional design method under the condition of the design head H_d=2.0m, flow rate Q_d=16.7*l*/min and rotational speed N_d=2230min^{-1} on the assumption that the mini centrifugal pump can be used for the cooling of electrical devices. Therefore, the specific speed is N_s=171 min^{-1}, m^3/min, m. The blade inlet angle of the original model was β_1=15° and the blade outlet angle was set as β_2=22.5° which was recommended by the conventional design method. However, it was difficult to obtain adequate head for the mini centrifugal pump with the open impeller because of the low Reynolds number effect and the leakage flow from a tip clearance [7]. Therefore, the large blade outlet angle β_2=60° was set as the base model to keep the head of the pump in this research under the condition that other design parameters were the same as those of the original model. Figure 1 shows schematic diagram and picture of the base model. Table 1 is the primary dimensions of the original and base rotor. The rotor has two-dimensional impeller and is made of the aluminum. The inner diameter of the rotor D_1=27mm, outer diameter D_2=55mm and blade width B=4.2mm. The suction diameter of the pump is D_{in}=26mm and its discharge diameter is D_{out}=13mm. The sectional view of the volute casing is rectangular and the inner diameter of the volute is 62mm. Therefore, the clearance at the volute tongue is 3.5mm because the outer diameter of the rotor is D_2=55mm.

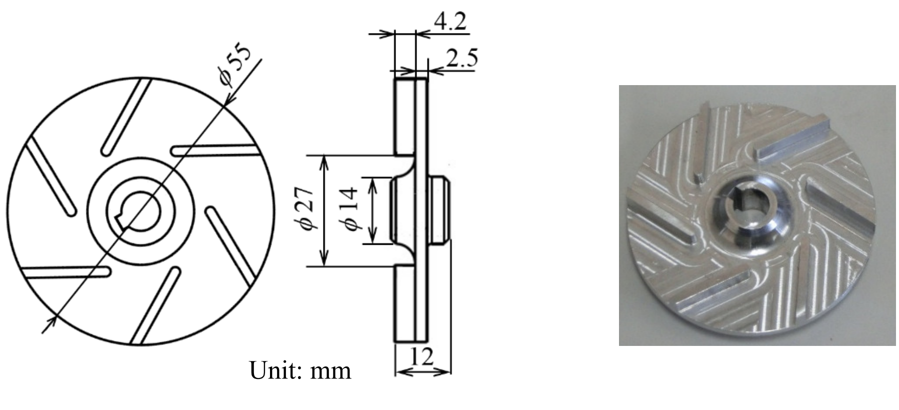

Figure 1. Test impeller for base model.

The schematic diagram of the experimental apparatus for the performance test is shown in figure 2. Water was used for the experiment. For the pressure performance evaluation, the static head difference on the wall between $2D_{in}$ upstream and $2D_{out}$ downstream of the rotor was measured by the pressure sensor Kyowa Electronic Instruments, PGM-1KG. Then, the pump total head was evaluated by adding the dynamic head difference of the sectional averaged axial velocity to the corresponding measured static head difference. The rotor was driven by the motor. The flow rate Q was obtained by a magnetic flow meter KEYENCE FD-UH25G installed far downstream of the pump and the torque was measured by a torque meter ONO SOKKI SS-010. The shaft power was calculated by the torque and rotational speed measured by a rotational speed sensor ONO SOKKI MP-981. The shaft power was evaluated by the torque eliminating the mechanical loss and disc friction loss using a disc without the impeller in this performance test. Then, the hydraulic efficiency of the pump η was calculated as the ratio of the water power to the shaft power.

Table 1. Primary dimension of rotors.

Geometry	Original model	Base model
Inlet diameter at hub D_{1h} [mm]	27	27
Inlet diameter at tip D_{1t} [mm]	27	27
Outlet diameter D_2 [mm]	55	55
Inlet width b_1 [mm]	4.2	4.2
Outlet width b_2 [mm]	4.2	4.2
Blade number Z [-]	6	6
Blade thickness s [mm]	2	2
Blade inlet angle β_1 [deg]	15	15
Blade outlet angle β_2 [deg]	22.5	60
Arc geometry	1Arc	1Arc

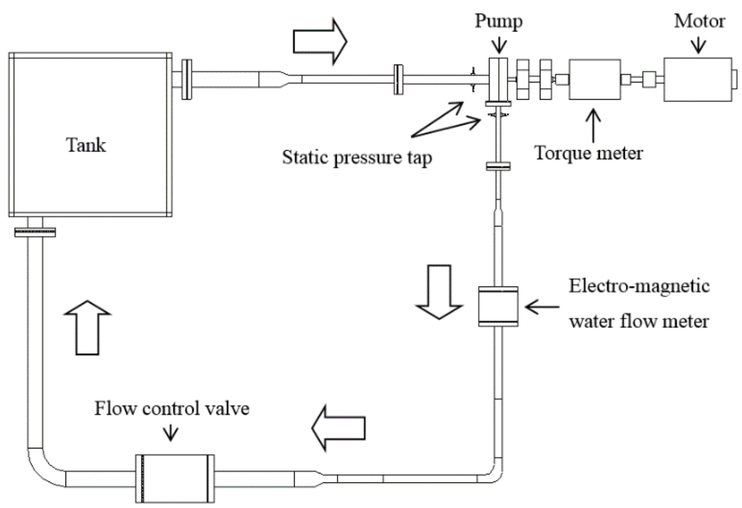

Figure 2. Schematic diagram of experimental apparatus.

2.2. PIV measurement instrument

The schematic diagram of PIV measurement instrument and test section for PIV measurement is shown in figure 3 and figure 4 respectively. FlowMaster Stereo-PIV by LaVision was used for PIV measurement. The test section was designed as same as the experimental apparatus for the performance test, the whole test section for PIV measurement was made of the acrylic resin including the test impeller in figure 5. The experimental apparatus for PIV measurement was a circulation water channel and the flow rate was controlled by a valve. Static pressure taps were set on the wall between $2D_{in}$ upstream and $2D_{out}$ downstream of the rotor and the pump total head was measured by the same method of the performance test. Then, the flow rate of the PIV measurement test was evaluated by the pump total head obtained by the PIV measurement and the head curve obtained by the performance test in section 2.1. The double pulse YAG laser with 135mJ power was used as a light source and double pulse timing widths(repetition rate) was set as 5μs (0.2MHz) considering the range of the measurement velocity. The phase locked averaged data were measured by inputting a trigger pulse from the rotor to PTU(Programmable Timing Unit). The measurement plane was axial sectional plane at the mid of the blade width b/B=0.5 near the volute tongue and its area was about 58mm×58mm because the calibration plate size was 58mm×58mm. Tracer particles were fluorescent particles EBM FLUOSTAR with particle diameter 15μm. Two CCD camera with its resolution 2048×2048 pixels were used and velocity vector and vorticity distribution were calculated by the PIV measurement software DaVis(Lavision).

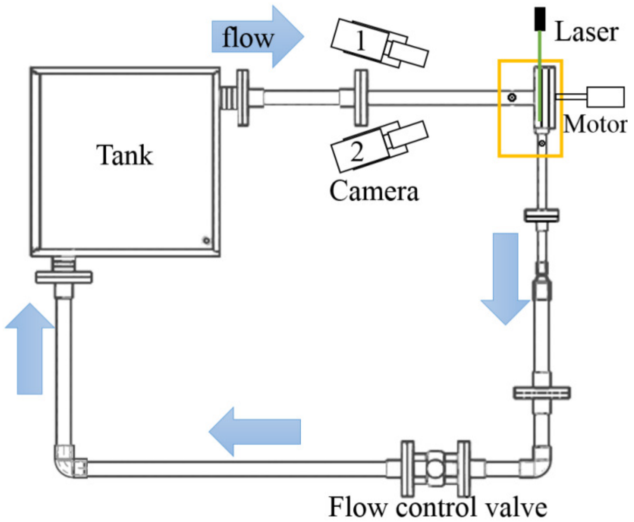

Figure 3. Schematic diagram of PIV measurement instrument.

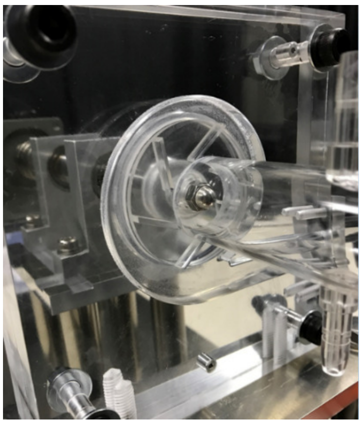

Figure 4. Test section for PIV measurement.

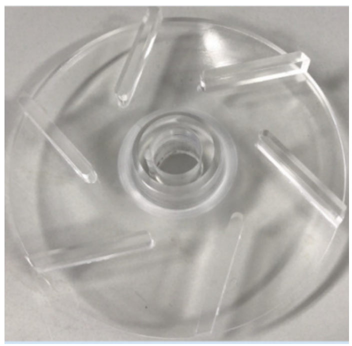

Figure 5. Test impeller for PIV measurement.

3. Numerical analysis condition

Numerical flow analysis was conducted to compare the internal flow obtained by the PIV measurement. In the numerical analysis, the commercial software ANSYS CFX16.2 was used and the numerical analysis was conducted with the three-dimensional model, which is the same with the test section of the mini centrifugal pump used in the performance test. Water was assumed to be incompressible and isothermal water and the equation of the mass flow conservation and Reynolds Averaged Navier-Stokes equations were solved by the finite volume method. The standard wall function was utilized near the wall and the standard k-ω model was used as the turbulence model. The computational grids used for the numerical analysis is shown in figure 6. The inlet of the numerical domain is $5D_{in}$ upstream of the test section and the outlet is $5D_{out}$ downstream of it. The constant velocity and constant pressure are given as the boundary conditions at the inlet and outlet respectively. The tip clearance is also made in the numerical analysis, which is the same with the experimental apparatus for the performance test and the number of elements within the tip clearance was 8. The numerical analysis was performed at 6 different flow rate points from 0.8-1.4Q_d. Grid point numbers of the inlet pipe, rotor region, casing region and outlet pipe region are 240,191 points, 4,376,568 points, 1,130,000 points and 266,179 points respectively, so the total grid points are 6,012,938 points. The unsteady numerical analysis was conducted and the coupling between the rotor and casing was accomplished by the sliding mesh(Transient Rotor Stator Model). The time step number per one rotor rotation is 180 and the time step is t=1.495×10^{-4} s. The data of one rotor rotation were obtained after 6 rotor rotations in unsteady numerical analysis.

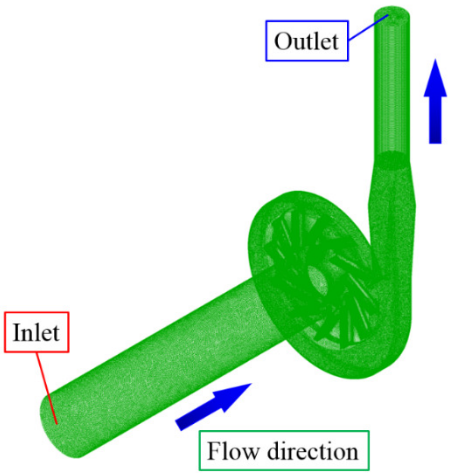

Figure 6. Numerical grids.

4. Result and discussion

4.1. Performance curve of the test mini centrifugal pump

Figure 7 shows the performance curves of the test mini centrifugal pump obtained by the experiment. The tip clearance is c=0.5mm and the performance test was conducted in wide flow rates range from the shut off flow rate to large flow rate in the experiment. Horizontal axis is the flow rate Q and first and second vertical axis of figure 7(a) is the head and shaft power respectively. The vertical axis of figure 7(b) is the efficiency η. The unsteady numerical analysis result is also shown in figure 7 to compare the numerical result with the experimental result. Focused on the head and efficiency curves of the experiment in figure 7, we obtained the head H=1.93m at the design flow rate Q_d=16.7l/min and the efficiency was η=56.5% at the same flow rate 1.0Q_d. The flow rate of the maximum efficiency shifts larger flow rate 1.2Q_d because the test rotor having the large blade outlet angle β_2=60°. The maximum efficiency is not so high, however, the relatively high head and efficiency are kept in large flow rate region. On the other hand, when we compared the numerical analysis result and experimental result, the numerical analysis results of head, shaft power and efficiency represented the qualitative

IOP Conf. Series: Earth and Environmental Science **240** (2019) 032026 doi:10.1088/1755-1315/240/3/032026

tendency of the experimental results and numerical analysis data of the performance accorded with the experimental data qualitatively for some data. Therefore, we concluded the unsteady RANS could capture the trend of the performance of the test mini centrifugal pump.

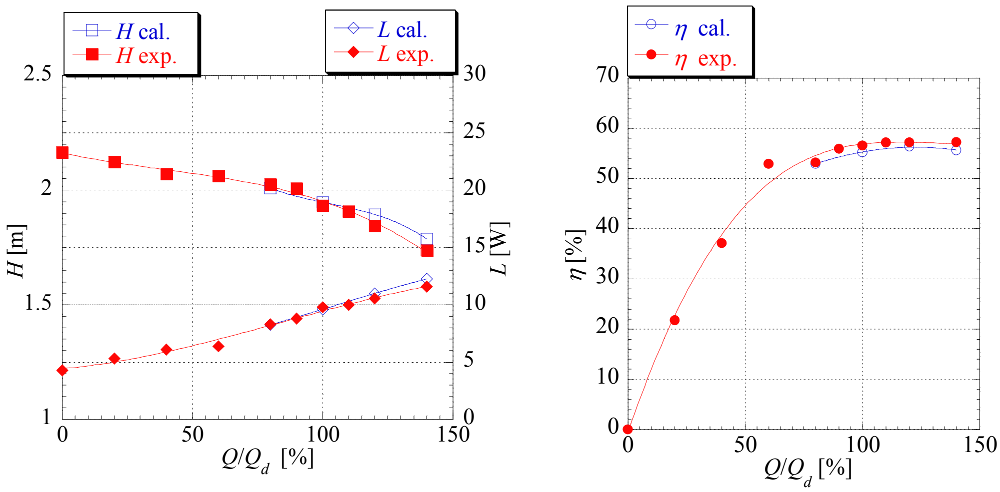

(a) Head and shaft power curves (b) Efficiency curve

Figure 7. Performance curves of test mini centrifugal pump.

4.2. Comparison between PIV measurement result and CFD result

In this research, we tried to focus on the flow condition near the casing tongue. It is difficult to validate the PIV measurement result using the other measurement technique because the test pump was small with 55mm rotor diameter. The performance of the test mini centrifugal pump could be captured well in figure 7, so we considered that the flow condition of the numerical analysis would show the adequate data of the internal flow for the test mini centrifugal pump. Then, we compared the PIV measurement result and numerical analysis result to investigate the validity of the PIV measurement results. The rotational position of the impeller is defined by the rotational angle of the trailing edge(TE) on the suction surface of the impeller from the casing tongue in figure 8. The anti-crock wise direction of the impeller is a positive for the rotational angle θ_r and its angle is zero when the TE on the suction surface of the impeller accords with the casing tongue. In order to compare the flow condition near the casing tongue, we defined the tongue flow angle α_t represented by figure 9. The sampling points for the data are 3mm away from the casing tongue and set at 0.5mm interval in

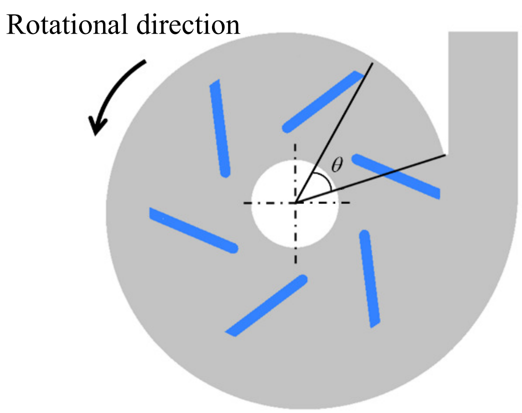

Figure 8. Rotational position of impeller.

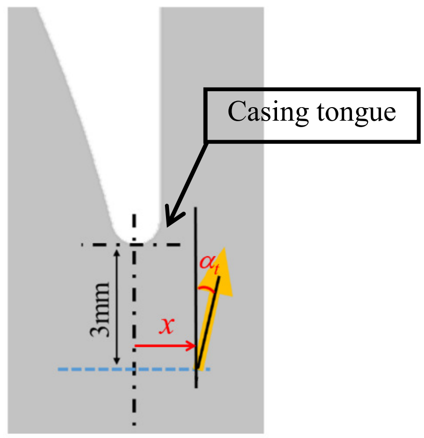

Figure 9. Definition of tongue flow angle α_t.

the horizontal line in figure 9. The center of the casing tongue is the origin x=0 mm and x is a positive in right direction in figure 9. The flow angle is the angle of the velocity vector from the vertical line in figure 9 at each sampling point and it is a positive in crock wise direction. The tongue flow angle at the design flow rate 1.0Q_d is shown in figure 10. The trend of the tongue flow angle distribution between the PIV measurement and numerical analysis is almost the same in the range -1.0mm < x < 1.0mm, however, there is some difference between them x < -1.0mm, 1.0mm < x. This difference may have occurred in RANS because it is difficult to reproduce the vortex and separation in the experiment. The value of the tongue flow angle is not so different each other and the tongue flow angle is minus in the region -2.0mm < x < 1.5mm for both case, which corresponds recirculation flow from the casing to the impeller at the design flow rate 1.0Q_d in the test pump. Therefore, we determined the PIV measurement results show the proper flow condition of the test mini centrifugal pump.

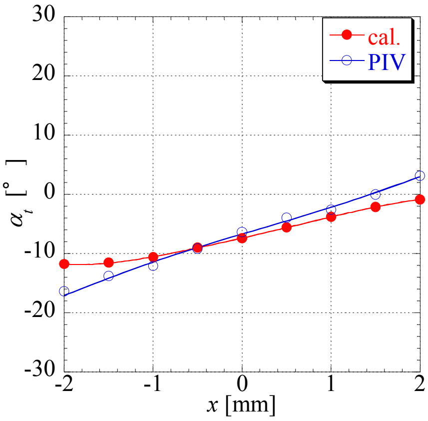

Figure 10. Tongue flow angle at design flow rate 1.0Q_d.

4.3. PIV measurement result

The absolute velocity vector overlapped with the velocity contours and the vorticity distribution at the design flow rate 1.0Q_d are shown in figure 11 and 12 respectively. The velocity vector shows the direction of the velocity and contour represents its magnitude. Anti-crock wise vorticity is a plus and crock wise vorticity is a minus in figure 12. The absolute velocity increases with the increase of the radial position and becomes high near the trailing edge on the suction surface of the impeller. The strong anti-crock wise vorticity occurs on the suction surface of the impeller because the test impeller has the large blade outlet angle β_2=60° and causes the separation on the suction surface of the impeller. In addition to that, the crock wise vortex shedding from the trailing edge of the impeller is induced and large slip is caused at the outlet of the impeller. When the trailing edge of the impeller approaches the casing tongue θ_r =0°, this vortex region from the trailing edge of the impeller is divided into two regions, volute inlet and discharge throat regions, and the strong interaction between the flow from the trailing edge and the casing tongue is generated.

The velocity vector and its contours at the partial flow rate 0.8Q_d is shown in figure 13. The absolute velocity at the radial outer region becomes larger than that at the design flow rate 1.0Q_d, which corresponds the increase of head at the partial flow rate in figure 7(a). The distribution of the velocity contours at 0.8Q_d is similar to that at 1.0Q_d, however, there is the difference of the magnitude of the velocity. Figure 14 shows the vorticity distribution at the same flow rate 0.8Q_d. Anti-crock wise vorticity is a plus and vice versa. The characteristics of the vorticity distribution at the partial flow rate 0.8Q_d, the anti-crock wise vorticity on the suction surface of the impeller, crock wise vortex shedding from the trailing edge of the impeller and interaction between the flow from the trailing edge and the casing tongue, are the same with that at design flow rate1.0Q_d. The vorticity magnitude at 0.8Q_d is smaller than that at 1.0Q_d, so the noise and vibration related to the vortex will be small at 0.8Q_d. The velocity vector and its contours at the large flow rate 1.4Q_d is shown in figure 15. The velocity at the radial outer region becomes small with the increase of the flow rate in figure 11, 13 and 15. The stagnation point on the casing tongue shifts the casing inlet side and causes the radially outer flow near the casing tongue, when the trailing edge of the impeller approaches the casing tongue θ_r =0°.

The vorticity distribution at the large flow rate 1.4Q_d is shown in figure 16. Anti-crock wise vorticity is a plus in figure 16. The magnitude of the vorticity on the suction surface of the impeller and vorticity shedding from the trailing edge of the impeller becomes larger with the increase of the flow rate as shown in figure 12, 14 and 16. The high vortex region on the suction surface of the impeller attaches on the suction surface at 1.4Q_d because the radial velocity increases with the increase

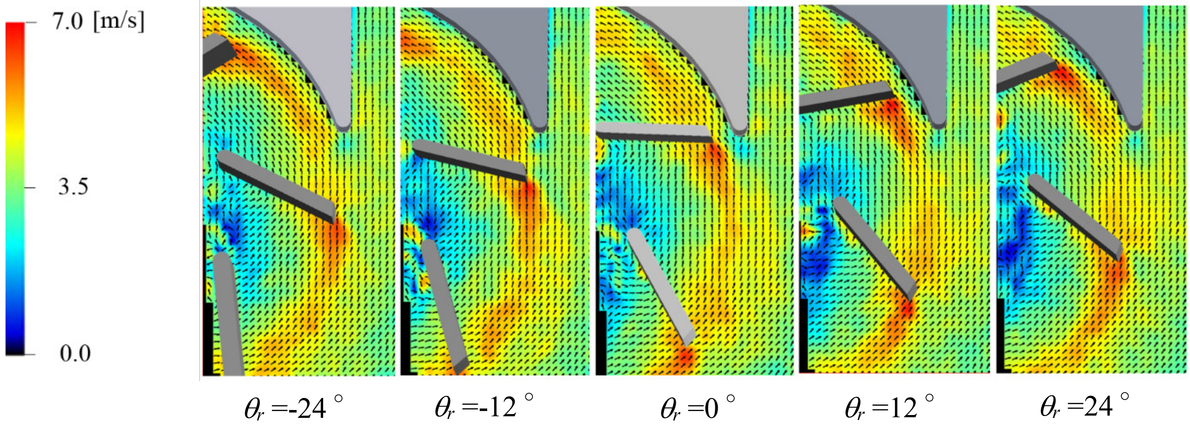

Figure 11. Absolute velocity vector overlapped with the velocity contours at design flow rate 1.0Q_d.

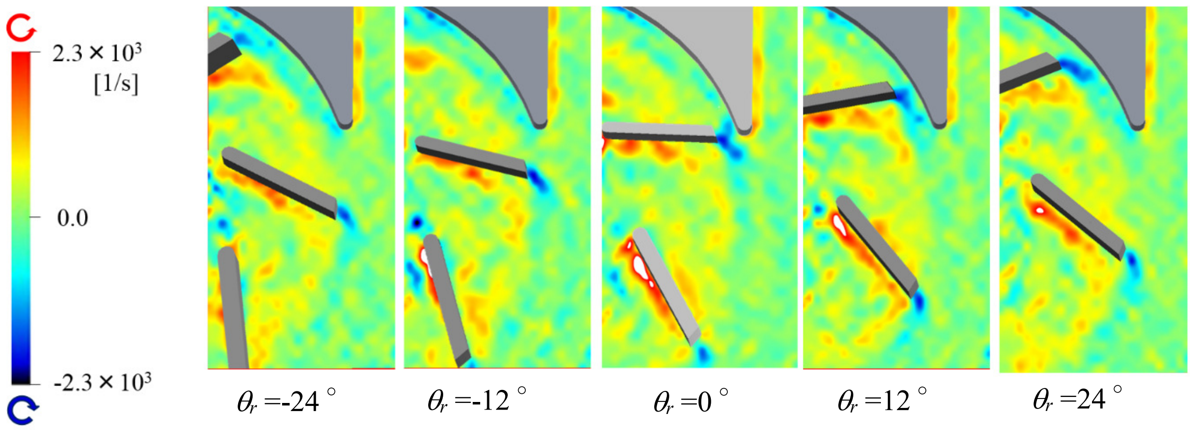

Figure 12. Vorticity distribution at design flow rate 1.0Q_d.

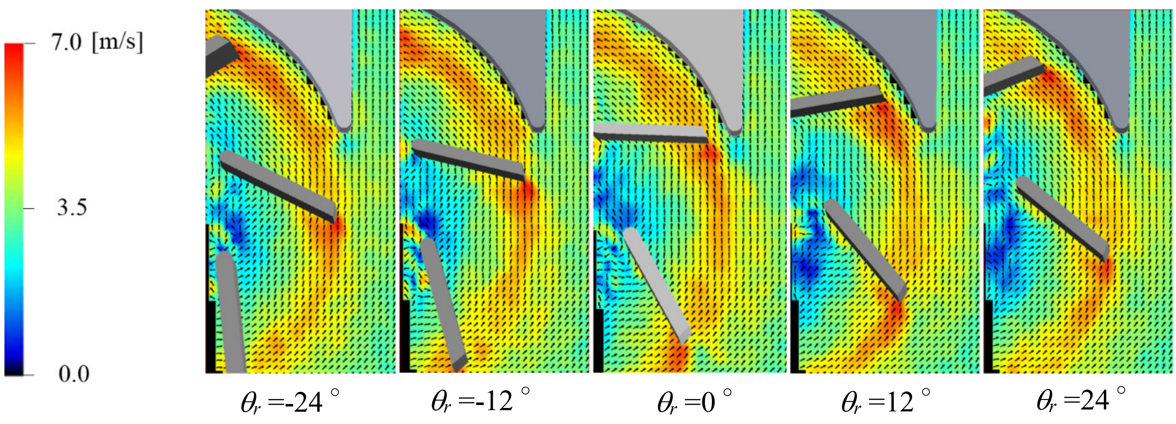

Figure 13. Absolute velocity vector overlapped with velocity contours at partial flow rate 0.8Q_d.

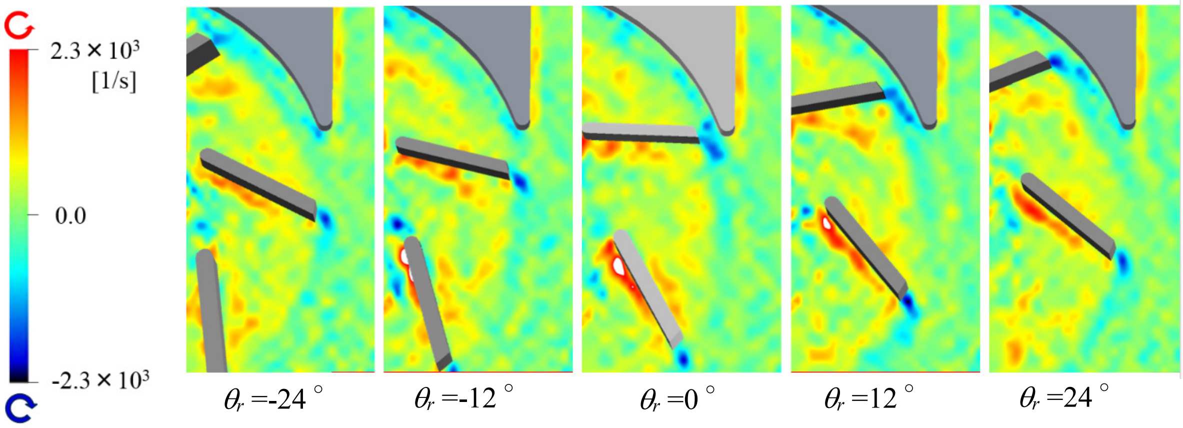

Figure 14. Vorticity distribution at partial flow rate $0.8Q_d$.

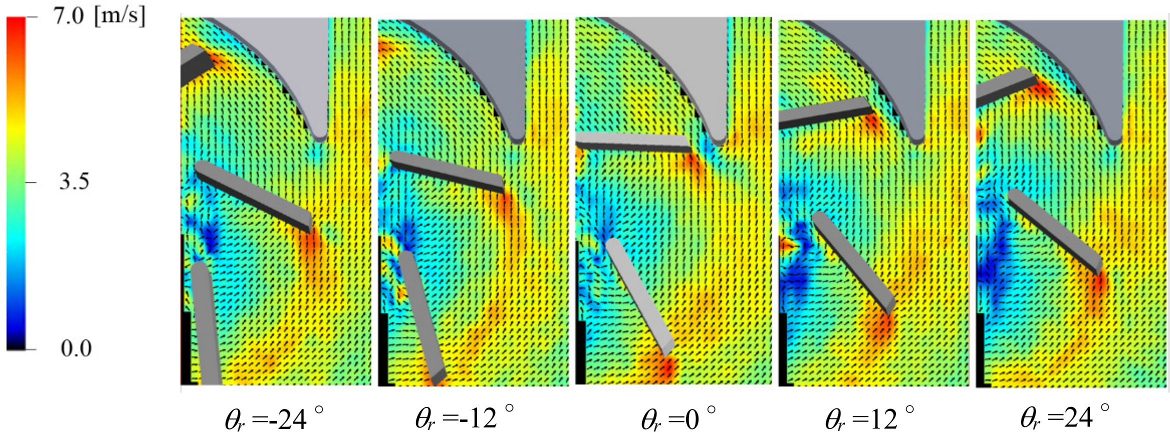

Figure 15. Absolute velocity vector overlapped with velocity contours at large flow rate $1.4Q_d$.

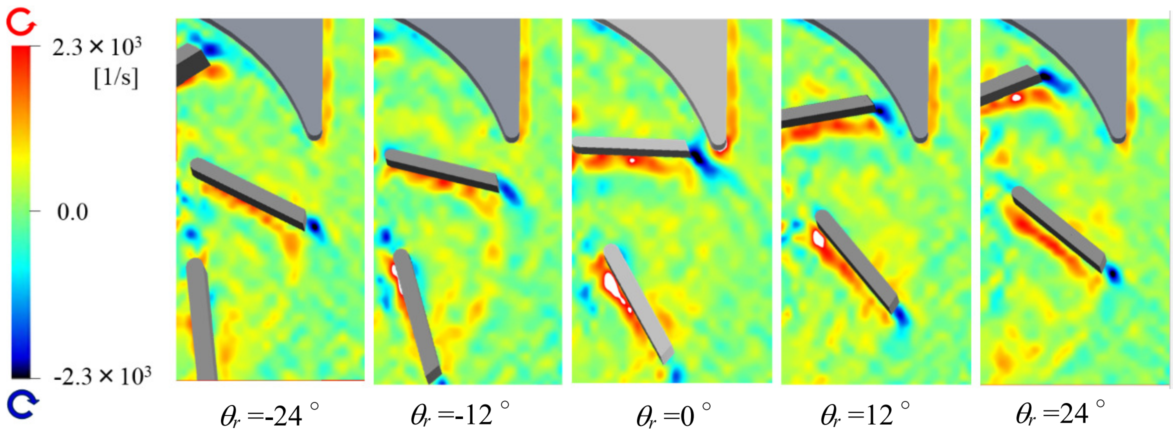

Figure 16. Vorticity distribution at large flow rate $1.4Q_d$.

of the flow rate and flow angle becomes large. The vorticity near the casing tongue shows the maximum value at θ_r =0° and vorticity near throat wall becomes large with the interaction between the flow from the trailing edge and the casing tongue.

5. Concluding remarks

The internal flow condition near the casing tongue of the mini centrifugal pump having large blade outlet angle β_2=60° was investigated by PIV measurement. The flow rate of the maximum efficiency shifts larger flow rate $1.2Q_d$ and the relatively high efficiency is kept in large flow rate region. The performance of the test mini centrifugal pump could be captured well by the numerical analysis. The trend of the tongue flow angle distribution between the PIV measurement and numerical analysis is almost the same in the range -1.0mm < x < 1.0mm. Furthermore, the value of the tongue flow angle is not so different each other and the tongue flow angle is minus in the region -2.0mm < x < 1.5mm for both case.

The strong anti-crock wise vorticity occurs on the suction surface of the impeller because the test impeller has the large blade outlet angle β_2=60°. In addition to that, the crock wise vortex shedding from the trailing edge of the impeller is induced and large slip is caused at the outlet of the impeller. When the trailing edge of the impeller approaches the casing tongue θ_r =0°, the vorticity near the casing tongue shows the maximum value and the strong interaction between the flow from the trailing edge and the casing tongue is generated. The stagnation point on the casing tongue shifts the casing inlet side and causes the radially outer flow near the casing tongue at the large flow rate 1.4Q_d, when the trailing edge of the impeller approaches the casing tongue θ_r =0°.

References

[1] Akamatsu T and Tsukiya T 1998 Development of a centrifugal blood pump with magnetically suspended impeller and the related fluid mechanical problems *Sadhana* vol 23 p 597-603

[2] Horiguchi H, Matsumoto S, Tsujimoto Y, Sakagami M and Tanaka S 2009 Effect of internal flow in symmetric and asymmetric micro regenerative pump impellers on their pressure performance *Int. J. Fluid Machinery and Systems* vol 2 p 72-79

[3] Shao J, Liu S, Yuan H and Wu Y 2008 Numerical simulation and PIV measurement on the internal flow in a centrifugal mini pump *Proc. Int. Conf. ASME Fluids Engineering Division Summer Meeting* FEDSM2008-55025

[4] Wu Y, Yuan H, Shao J and Liu S 2009 Experimental study on internal flow of a mini centrifugal pump by PIV measurement *Int. J. Fluid Machinery and Systems* vol 2 p 121-126

[5] Keller J, Blanco E, Barrio R and Parrondo J 2014 PIV measurements of the unsteady flow structures in a volute centrifugal pump at a high flow rate *Experiments of Fluids* vol 55 1820

[6] Zhang J, Wang Y and Yuan S 2015 Experimental research on internal flow in impeller of a low specific speed centrifugal pump by PIV *Proc. the 13th Asian Int. Conf. on Fluid Machinery* AICFM13-147

[7] Shigemitsu T, Fukutomi J and Nasada R 2009 Study on performance and internal flow condition of mini turbo-pump *Proc. the 10th Asian Int. Conf. on Fluid Machinery* AICFM112

[8] Nishi M, Liu S, Yoshida K, Tsukamoto H and Kouya S 1998 Tip-clearance effect on the performance of a high speed mini turbopump *Proc. The Third Int. Conf. on Pumps and Fans* p 223-231

[9] Liu S, Nishi M, Yoshida K and Tsukamoto H 2000 A study on a high speed mini turbopump(2nd rep: Effect of bypass flow on the pump performance *Proc. 2nd Symp. on Fluid Machinery and Fluid Engineering* p 633-636

[10] Liu S, Nishi M and Yoshida K 2001 Impeller geometry suitable for mini turbo-pump *ASME J. Fluids Engineering* vol 123 p 500-506

[11] Choi Y, Kurokawa J and Matsui J 2006 Performance and internal flow characteristics of a very low specific speed centrifugal pump *ASME J. Fluids Engineering* vol 128 p 341-349